

THIS FILE IS UNDER FORMATTING, AS THE PDF IS READY FILE WILL BE REPLACED

Axial Compression Behavior of Aluminum (Al), Glass/Epoxy (GFRP) and Hybrid Al-GFRP Crash-box: An Experimental and Digital Image Correlation Approach

Varsha M.P.¹, Mahesh², Prashant Rawat^{2}*

¹ Department of Mechanical Engineering, National Institute of Technology, Tiruchirappalli - 620015 Tamil Nadu, India.

² Department of Aerospace Engineering, Indian Institute of Technology Madras, Chennai - 600036 Tamil Nadu, India.

Abstract

The study aims to understand the axial compression characteristics and fracture of cylindrical Aluminum (Al), Glass/epoxy (GFRP) composite and Hybrid Al-GFRP crash-boxes. The hollow Al tubes are fabricated by rolling and bonding a thin aluminum sheet followed by rivet joints. The GFRP samples are manufactured using the wet-hand layup technique followed by the vacuum bagging method. Hybrid samples are manufactured by covering GFRP tubes with aluminum sheets on the outer and inner sides bonded by commercial Araldite[®]. The prepared samples are axially compressed in a universal testing machine (UTM). The strain field study by the Digital Image Correlation (DIC) technique is performed to identify the possibility of fracture modes in the prepared crash boxes. The continuous damage progression is measured using acoustic sound signatures. It is observed from the experimental results that the Al-GFRP samples showed the highest load carrying capacity. The GFRP composites showed the highest specific energy absorption (SEA) and a relatively stable axial crushing phenomenon. The comparative results proved that DIC and acoustic analysis can accurately identify the fracture in hollow crash-boxes (without physical contact and causing damage in the samples) during the experiments.

Keywords: Axial compression; GFRP; Hybrid crash-box; Crashworthiness; Failure Modes, DIC; Acoustic analysis; Non-contact fracture analysis.

*Corresponding Author: prashant.rawat@iitm.ac.in

INTRODUCTION

In the automobile industry, there is an increasing demand to improve the crash protection and efficiency of its structures. The crash box is an energy absorbing structural member placed in the anterior section of a vehicle to absorb impact energy. During accidents, the crash box experiences compressive deformation followed by predictable and stable crushing without transferring impact energy to the interior components. From the design point of view, the frontal structure of an automobile body can be subdivided into three load paths (i) Load path 1: contains bumper beams, crash boxes and longitudinal beams as shown in Fig. 1a, (ii) Load path 2: contains upper rails or reinforcements (hood ledge), pillars and (iii) Load Path 3: includes Sub-frames and cradles, Sill beams or reinforcements^{1,2}. Application of crash boxes includes stagecraft devices, gearboxes, automobile bumper beams, floor substructures, wing panels in the aerospace sector, etc.

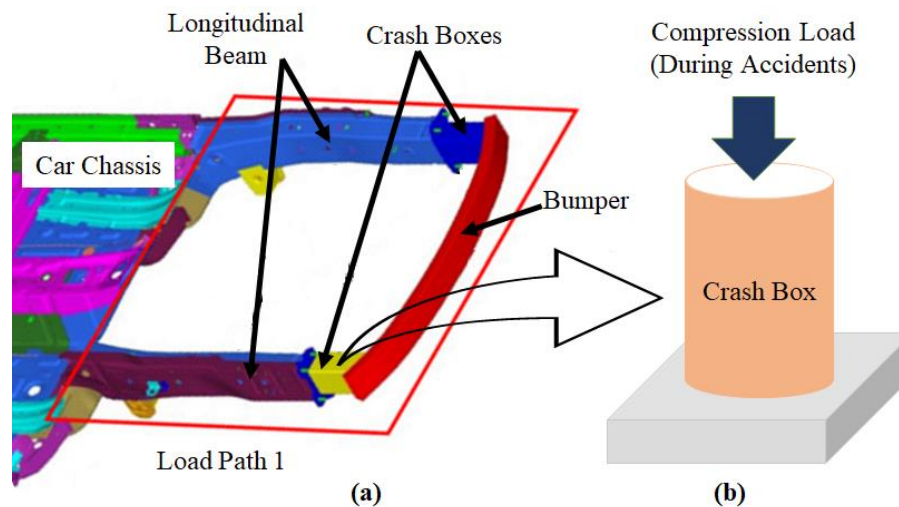


Fig. 1: Schematic representation of (a) an automobile's frontal structure and (b) crash-box position.

Thin walled tubes are the most commonly preferred designs used in crash boxes, which show stable, larger plastic deformations and absorb incident energy under axial compression loadings. Therefore, earlier studies have focused on identifying the most suitable materials for a stable and progressive folding under axial-compressive loads. Aluminum, fibre polymer

composites (carbon fibre, glass fibre, etc.), and foams filled tubes are the most popular choice among materials to effectively absorb and dissipate energy. They also minimize damage to the surrounding components. In addition, cross-section columns with various shapes, such as square, circular, and rectangular, with different thicknesses are also well investigated ³. Investigations on the comparative performance of composite and metallic crash-boxes showed that composite crash-boxes show almost 1.5 times better performance in terms of impact energy absorption ². Moreover, cylindrical tubes (made of glass, Kevlar, and carbon polymer composites) show more stable properties than square and rectangular tubes ⁴.

The sandwich composites combining various polymer composites and metals are an interesting and economical choice to improve crashworthiness ⁵. This combination also provides better mechanical properties (specific energy absorption) than metal and FRP crash-boxes under axial loading ⁶. In hybrid combinations, multiple layups are possible using the metal tube inner wall (inside), or outer wall (outside) or between the FRP layers. Different combinations with variations in the thicknesses of each constituent of materials may lead to variations in failure modes and energy absorption capabilities ⁷⁻¹⁰. The majority of these conducted studies focus on the crashworthiness of a design in identifying the energy absorption using controlled failure mechanisms and modes ¹¹. This can be done under two types of loading conditions (i) Quasi-static loading and (ii) Impact (dynamic). The controlled failure mechanism under quasi-static load conditions allows gradual deterioration of the tested specimen's profile and provides significant time to study the material response. Therefore, it is well investigated in the last three decades. Most of the time, the crashworthiness is analyzed by experimental analysis where partial or complete fracture of sample takes place.

In-situ capturing of failure modes in composites during axial compression is difficult. However, recent developments in non-contact type strain measurement techniques, such as digital image correlation (DIC) have shown promising results for capturing in-situ deformations and fracture during the experiments ^{12,13}. The DIC technique is based on examining the strain-fields (movement of multiple points with respect to each other) in the samples. This technique can also provide stress concentration zones (potential fracture spots), crack initiation and propagation behavior. Another non-contact method to capture the in-situ failure mode is the acoustic technique. In the acoustic technique, the sound signatures produced by the specimens during the testing are captured and correlated to the failure modes. This method is particularly useful for composite materials, as they produce sound signatures during axial crushing tests in matrix, delamination and fibre fracture.

Interestingly, several experimental and numerical investigations have been done to address different aspects of composite crash-boxes, which proved the importance of understanding the crushing behavior of hybrid crash-boxes under axial compression loading. This study attempts to add the existing knowledge with the implication of digital image correlation (DIC) along with acoustic analysis in axial compression loading for three different samples (i) Al sheet-based tubes, (ii) GFRP tubes, and (iii) Sandwich Al/GFRP tubes (GLARE) under quasi-static loading conditions. The load response, specific energy absorption (SEA) and fracture analysis of samples are compared to identify the most suitable design for the crash box.

EXPERIMENTATION

The cold rolled thin aluminum sheet of thickness 0.5 mm was acquired from the local market. A 400 GSM glass fibre with bidirectional and plain weaving fabric architecture was used as reinforcement, which was supplied by Fibre Region, a local supplier from Chennai, India. The Bisphenol-A-based resin (Araldite[®] LY 556) and amine based (Aradur H951) hardener were obtained from Javanthee Enterprises in Chennai, India. The same resin material was employed as a matrix material for manufacturing GFRP tubes. A commercially available two part adhesive Araldite[®] (HW 106) and hardener (HV953) was used to prepare the GLARE tubes.

A plain woven fabric was cut from the parent roll to fabricate a GFRP tube with a 1:1 aspect ratio (diameter: height). After mixing epoxy resin and hardener by weight (1: 10 ratios, as suggested by the supplier), glass woven was brushed with the resin and rolled over a PVC pipe of diameter 75 mm. The PVC pipe was cleaned with acetone and ethyl acetate. After that a mold releasing agent was sprayed and left for drying. After rolling, the wet laminate was kept inside the vacuum bag and applied a pressure of 550-600 mmHg till the air inside the bag was removed entirely. Finally, the GFRP tubes were allowed for curing at room temperature for 24 hours. After the curing of the GFRP tubes, an aluminum sheet (75 mm wide) was adhered to the outside surface of the cured GFRP tubes using the Araldite[®]. After curing, the aluminum sheet was pasted inside the cured GFRP specimen. In this manner, the GLARE specimens were prepared. Similarly, the aluminum tubes were also prepared. However, the aluminum tubes were additionally reinforced with five rivets (at uniform distances) to avoid bond failure during the testing. Fig. 2a-c indicates the fabrication process of crush boxes.

The fabricated aluminum, GFRP, and GLARE tubes were axially crushed at 1 mm/min crosshead using universal testing equipment (Fig. 2d). The load vs. displacement curves were acquired and analyzed for various mechanical characteristics. A portion of the specimen was

captured during the axial crushing for DIC analysis. Sony Alpha 7 DSLR camera with a 75 mm lens was used for recording the testing. A light source was used for better surface exposure during the testing. The Sony Alpha 7 has an inbuilt microphone (ECM-CG50/XLR-K1M). Thus, the captured video recordings were post-processed for acoustic sound signatures. The audio recordings were post-processed using an open source software called Audacity^{14,15}. All the noises in the video recordings were removed during the post-processing to highlight the matrix cracking, delamination, and fibre fracture that occurred in the composite tubes during the axial crushing.

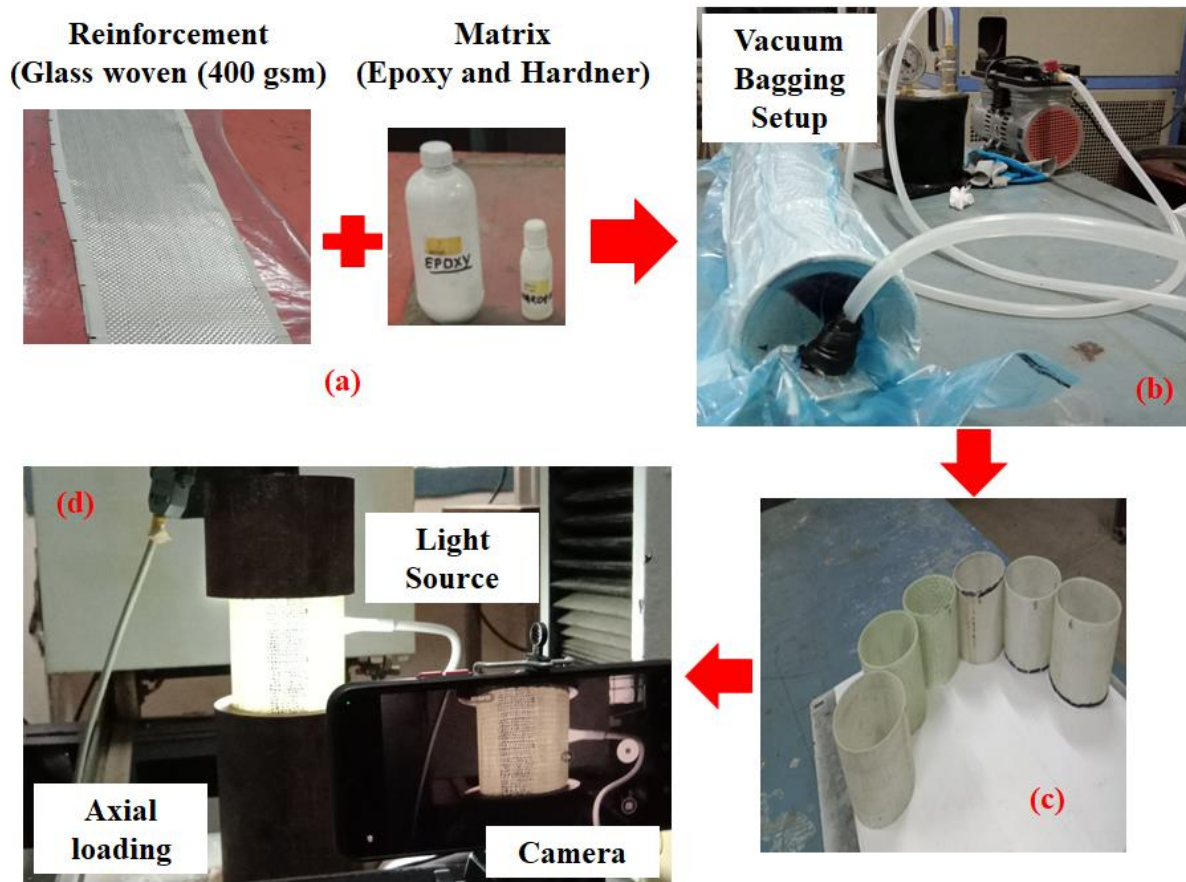


Fig. 2: Fabrication process: (a) constituent materials, (b) vacuum bagging setup of (c) GFRP cylindrical tubes and (d) testing under axial crushing loading.

RESULT AND DISCUSSION

LOAD VS. DISPLACEMENT BEHAVIOR

The load-displacement behavior of Al, GFRP and Al-GFRP samples are shown in Fig 3a-c. All three samples are axially compressed at 1 mm/min crosshead speed from the top side until the sample load behavior is saturated. In Fig 3a, thin aluminum tubes showed progressive folding

with a peak load of 17.21 ± 21 kN (shown in Fig 4a). The failure for this sample began at the bottom side, and folding propagated towards the top side with a constant decrease in load (see Fig 3a). GFRP samples showed relatively better crashworthiness metrics and increased load capacity with a peak load of 23.67 kN, which is 37.54% more than the thin aluminum tubes. The GFRP specimens failed by opening and crushing as the load on the GFRP tubes increased. It showed no sudden drop in the load after reaching the peak load. As observed in aluminum tubes, the GFRP tubes showed no folding failure. Instead, continuous fluctuations in the load vs. displacement are observed, indicating progressive failure. The load vs. displacement curves of tested GFRP specimens are more scattered than the aluminum specimens due to their heterogeneity and anisotropy. The load variations with respect to the displacement also fluctuated after reaching the peak value. Curves of the tested samples are similar except for GFRP (1) samples, which showed relatively lower load characteristics. This behavior could be due to delamination or matrix rich section (non-homogeneity), which might lead to the earlier failure.

The hybrid Al-GFRP samples showed the best load carrying features among all three cases. The peak load attained by the GLARE sample is 40.08 ± 2.7 kN, and the failure pattern (after peak load) is similar to GFRP samples. The peak load of Al-GFRP samples is 137% more than the aluminum specimens and 72% more than the GFRP specimens. Overall, the load behavior is better for GFRP and Al-GFRP (or GLARE) samples, where crushing occurred predictably (in steps). Further, both samples showed no signs of catastrophic failures (see Fig 3d). The progressive failures are observed in the form of fibre, delamination and matrix failure in acoustic recordings (inset Fig 3b-c). Important conclusions that can be drawn from this analysis are that the failures in GLARE samples are relatively higher, which will be discussed in the upcoming section.

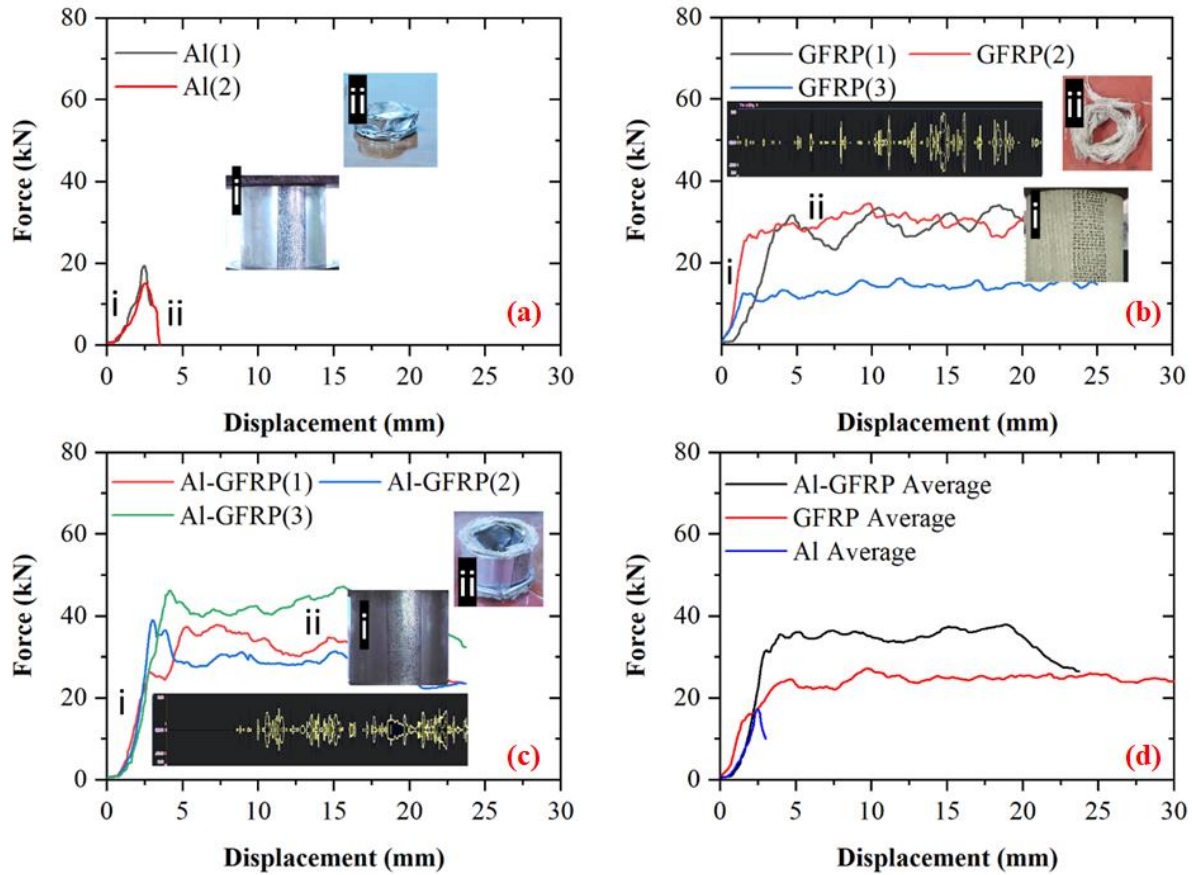


Fig. 3: Force vs displacement curves under axial compression loads for (a) aluminum, (b) GFRP and (c) GLARE crash-box with undamaged and damaged samples and acoustic results and (d) comparative analysis.

SPECIFIC ENERGY ABSORPTION

The geometry (tube shape and inner diameter) is constant for all three samples. However, the variations in thickness of tested samples were in the range of ± 1.2 mm. Therefore, the specific energy absorption (SEA) parameter is considered to identify the best among the three specimens. The SEA is calculated by dividing the area under the force vs. displacement curve with the specimen's weight. Fig. 4a-c summarized the comparison of SEA of tested specimens. Considering the Al sample as a reference, the SEA of GFRP and GLARE samples are 13.85 ± 4.09 and 8.52 ± 0.9 g/mm². These values are significant and prove that samples made of GFRP materials are best regarding the SEA and failure patterns. In addition, GFRP also showed significant variations in the load carrying capacity and SEA than the other two samples. Overall, the SEA of the GFRP sample is 3047 times higher as compared to Al tubes and 38 times higher than the GLARE sample.

Previous investigations have also reported this behavior for Al, GFRP and metal/FRP hybrid crash-boxes¹⁶. The SEA results for hybrid tubes are lower than composite tubes, and the reason for this behavior is density variations¹⁷. However, many other parameters like crash-box geometry, stacking sequence, tube thickness, and ply angle are critical parameters to measure the crashworthiness of designs in composites or hybrid combinations^{16,18}.

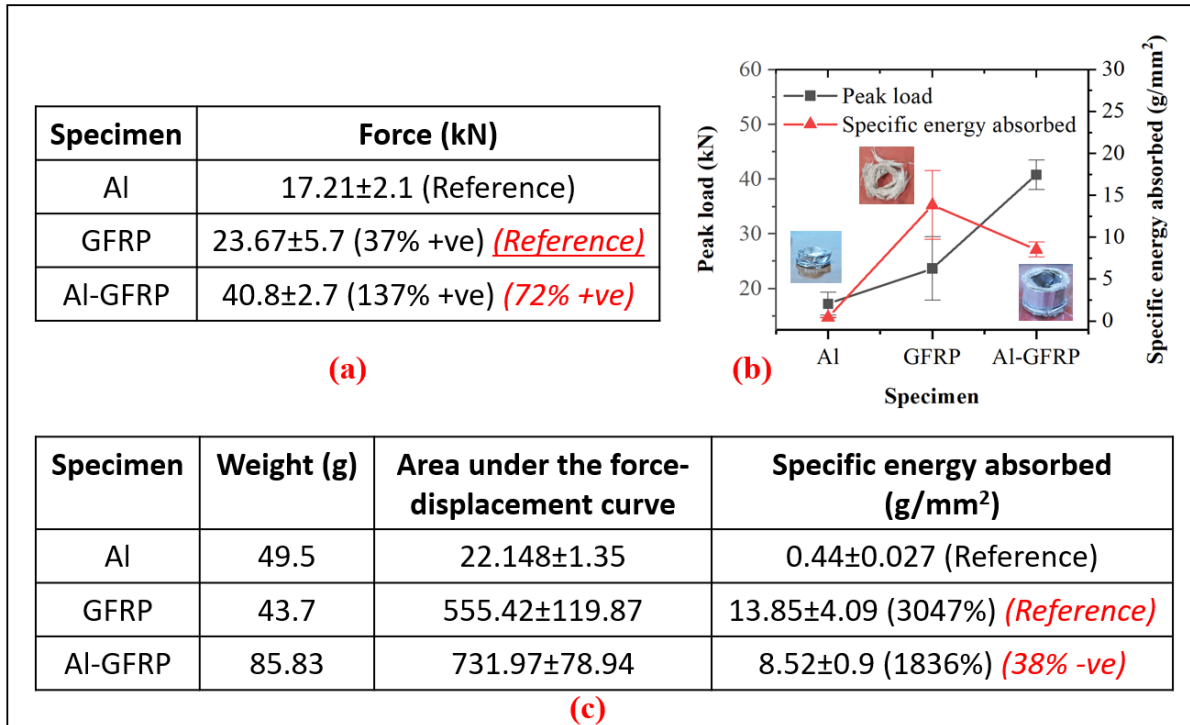


Fig. 4: (a) Peak force values with (b) comparative analysis for specific energy absorption and (c) relative improvements in SEA for Al, GFRP and Al-GFRP (or GLARE) samples.

AXIAL COLLAPSE AND DAMAGE PROPAGATION

A general understanding established from the experimental analysis is that the Al samples collapsed under plastic deformations followed by in-out folding (see Fig 5a). The GFRP tubes resulted in progressive failures throughout the sections and collapsed completely. The tested samples are broken entirely into several fragments with a stable deformation pattern (based on load response curves). Additionally, using DIC analysis, it has also been observed that the strain fields recorded in GFRP samples were symmetric in nature with respect to vertical and horizontal planes (see Fig 6a-c). Samples with Al-GFRP combinations also showed stable deformations with bond failure outside Al-covering after reaching the peak load. The mid layer of GFRP in the hybrid sample broke into several small fragments. Interestingly, the inner layer of the Al-sheet progressively folded at the top and bottom sides (very similar to the Al-tube).

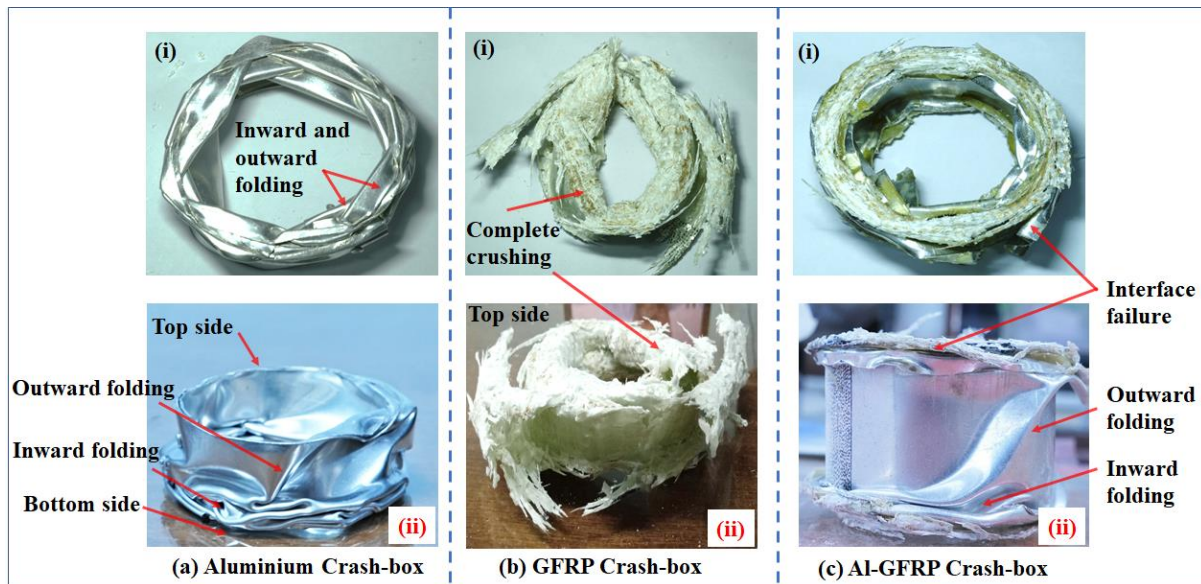


Fig. 5: Modes of collapse for (a) Al, (b) GFRP and (c) Al-GFRP (or GLARE) crash-box.

DIC AND ACOUSTIC ANALYSIS

The non-contact optical technique, such as digital image correlation (DIC) is used to monitor and analyze the deformation, displacement, and strain fields of objects exposed to mechanical stresses. This non-contact strain measurement technique adequately measures tube displacement and strain fields under axial compression¹⁹. As shown in Fig 3a-c (inset), the movement of small subsets or patterns is recorded and analyzed for strain and displacement fields. Fig 6a-c illustrates the strain fields in x-, y- and xy-plane (xy is a shear plane), and 6d-e represents the deformation in the x-, and y-directions. The strain and displacement fields are calculated using MATLAB open-source code by Ncorr^{20,21}. The strain fields along the x-direction in Al samples showed variations in the mid and final stages at the right-bottom section, which is the stress-concentration location. After reaching this stage, the Al sample started folding inward and outward directions (at the tube's bottom section). The validation of this behavior can be seen in Fig 6e-f, where a negative strain field (indicated as a blue spot) is visible and proves the inward folding of the Al-sample at this point. The strain fields exhibited an interesting symmetrical pattern (at half-height plane) of the sample (see Fig 6a-b). In the final loading stage, strain fields at the mid-section (in the horizontal plane) are relatively high. The reason for this phenomenon is the crushing of GFRP tubes on both sides (top and bottom), which released stresses in both points. The U and V patterns of GFRP samples are positive and uniform, indicating that the crushing occurred only at the top and bottom sections of the tubes without deforming the shape of the GFRP samples. It also shows a stable crash or collapse of the GFRP sample. Strain fields for Al-GFRP samples are similar to Al-samples from the outside

(where symmetry existed in the vertical plane) and clearly indicate that outer covering with Al sheet dominated in reacting to the applied load. Interestingly, post analysis of the samples showed that the Al-GFRP samples failed in mixed modes where the outer and inner layers of Al sheet collapsed and folded in- and out-direction at the top and bottom sections of the tubes. Whereas, the GFRP core collapsed and broke into several fragments at the top and bottom sides.

The strain fields along the xy-direction are lower than the x-direction. The shear strain fields are higher in Al specimens compared to the Al-GFRP specimens followed by GFRP specimens. Shear strain fields are lower in GFRP specimens than in Al and Al-GFRP specimens. The shear strain fields in both Al and Al-GFRP specimens are highly concentrated at the ends of the specimens, while the GFRP specimens showed more even distribution in the shear strain fields. The strain fields along the y-direction are also higher for Al specimens compared to the GFRP and Al-GFRP specimens. The U- and V-deformations showed a negative fold in hybrid samples, indicating fold-failure at both ends of the sample, similar to the Al-tube.

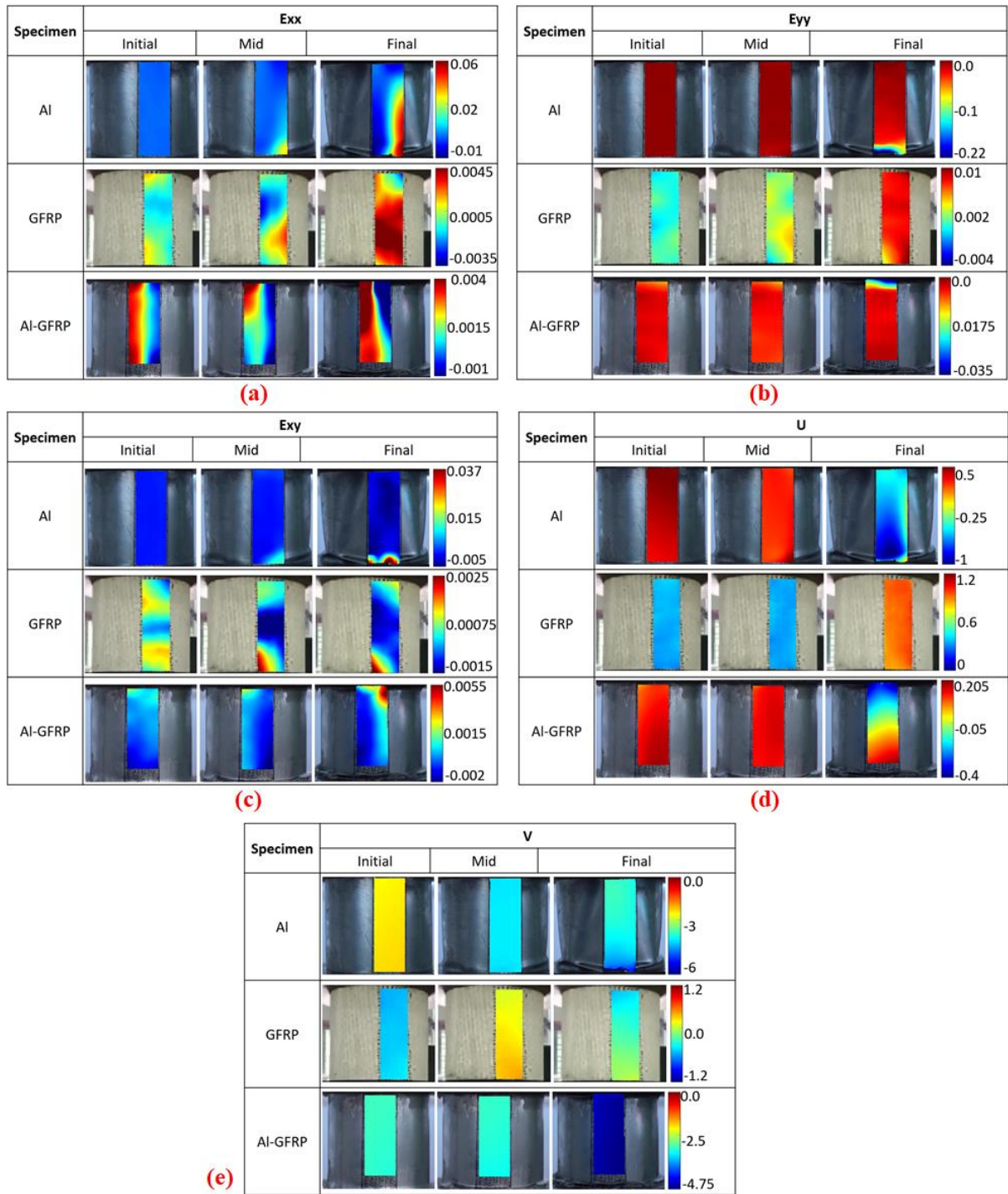


Fig. 6: Digital image correlation analysis for strain fields of Al, GFRP and Al-GFRP (or GLARE) samples in (a) X-, (b) Y-, (c) XY- direction and out- and inward-direction deformations in the transverse direction to the loading.

The acoustic patterns for the GFRP and Al-GFRP samples are shown in Fig 7. The vertical fringe (lines) indicates the cracking sounds representing the matrix cracking, delamination and fiber fracture in GFRP samples. The GFRP failure pattern is distributed uniformly (relatively),

and the failure intensity (closeness of fringes) increases with time. This indicates that the initial fracture can be delamination where the top and bottom sections of the sample are delaminated. Gradually, with the increase in loading, the sound intensity increased, which indicates that delamination followed by fiber fracture occurred in the GFRP tubes. After a certain level of loading, the noise reduced with lesser intensity, indicating more minor fractures in the final stage before the GFRP sample collapsed completely.

The Al-GFRP tubes did not show any failure initially because the Al-layers on both sides carried the load. This phenomenon can also be verified by DIC strain patterns for hybrid tubes where initially, Al-layer folding took place on the top and bottom sides of the loaded sample. The noise intensity for the Al-GFRP sample is relatively dense due to the interface failure of the Al sheet and GFRP core. In addition, the collapse of the GFRP core did not occur freely; as a result, cracking noise continued due to the collapse of the GFRP core within closed boundaries.

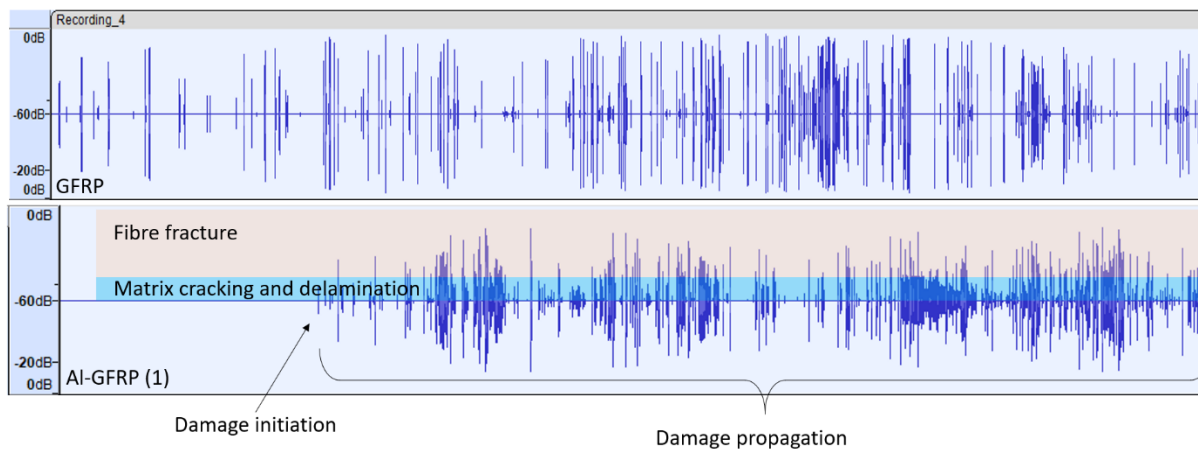


Fig. 7: Acoustic analysis for GFRP and Al-GFRP (or GLARE) crash-box.

CONCLUSION

This experimental work investigated the behavior of Al, GFRP and Al-GFRP tubes under axial compression loading. The digital image correlation technique is used to examine the strain fields and displacement fields. Further, the acoustic signatures are also examined to correlate the damage initiation and propagation in the specimens under axial compression loading.

- The Al-GFRP tubes showed the highest peak load compared to Al and GFRP tubes. However, the specific energy absorbed by the GFRP tube is higher compared to the Al and Al-GFRP tubes. Further, continuous damage propagation after reaching the maximum peak load is observed in GFRP and Al-GFRP tubes, whereas no such damage

propagation is observed for Al tubes. The Al tubes failed by folding and local buckling, whereas the GFRP and Al-GFRP tubes failed by outward opening and crushing without the folding mechanism. Moreover, the Al and Al-GFRP tubes failed by rolling mechanism. The specific energy absorption of the GFRP composite sample is 3047 times higher as compared to Al metal tube and 38 times higher than the GLARE or hybrid (composite core sandwiched with metal sheet) samples.

- The digital image correlation captured the stress concentration in Al, GFRP, and Al-GFRP tubes under axial compression. The strain fields along x-, y-, and xy-directions are higher for Al tubes, followed by Al-GFRP and GFRP tubes. The strain is distributed uniformly in GFRP tubes, whereas a high concentrated strain zones are observed in Al and Al-GFRP specimens at the junction of the specimen and loading end. Further, the GFRP specimens showed lower deformation than the Al-GFRP and Al tubes due to the higher stiffness of the GFRP specimen.
- It is evident from the acoustic analysis that the damage initiation in GFRP tubes is earlier than in the Al-GFRP tubes. However, the damage progression is uniform in both GFRP and Al-GFRP specimens after damage initiation. Furthermore, the intensity of acoustic signatures corresponding to the fibre breakage are reduced in Al-GFRP compared to the GFRP specimens due to the presence of Al.

It is also evident that the digital image correlation and acoustic signatures can effectively provide the strain fields, displacement fields and acoustic signatures. Further, the digital image correlation can be extended effectively for capturing the 3D strain fields as a future work for a better understanding of FRP tube failure under axial compression loading. This will also highlight full strain field (complete surface of crash box) and identify the collapse (crack initiation and propagation) steps in a crash-box.

REFERENCES

1. Wang G, Zhang Y, Zheng Z, Chen H, Yu J. Crashworthiness design and impact tests of aluminum foam-filled crash boxes. *Thin-Walled Structures*. 2022;180:109937.
2. Choi S-y, Hong S-c, Park S-k, Jeong S-w. Effects of Diameter-to-thickness Ratio on Impact Energy Absorption Capability of CFRP Cylindrical Crash Box. *International Journal of Automotive Technology*. 2022;23(6):1663-1671.
3. Nasir Hussain N, Regalla SP, Daseswara Rao YV. Study on influence of notch triggers on absorption of energy for composite automobile crash box under impact loads. *Materials Today: Proceedings*. 2021/01/01/ 2021;38:3220-3231. doi:<https://doi.org/10.1016/j.matpr.2020.09.715>
4. Thornton PH, Edwards P. Energy absorption in composite tubes. *Journal of Composite Materials*. 1982;16(6):521-545.
5. Yang H, Lei H, Lu G, Zhang Z, Li X, Liu Y. Energy absorption and failure pattern of hybrid composite tubes under quasi-static axial compression. *Composites Part B: Engineering*. 2020;198:108217.
6. Zhu G, Sun G, Yu H, Li S, Li Q. Energy absorption of metal, composite and metal/composite hybrid structures under oblique crushing loading. *International Journal of Mechanical Sciences*. 2018;135:458-483.
7. Zhu G, Sun G, Li G, Cheng A, Li Q. Modeling for CFRP structures subjected to quasi-static crushing. *Composite Structures*. 2018;184:41-55.
8. Özen İ, Gedikli H, Aslan M. Experimental and numerical investigation on energy absorbing characteristics of empty and cellular filled composite crash boxes. *Engineering Structures*. 2023;289:116315.
9. Wierzbicki T, Abramowicz W. On the crushing mechanics of thin-walled structures. 1983;
10. Shin KC, Lee JJ, Kim KH, Song MC, Huh JS. Axial crush and bending collapse of an aluminum/GFRP hybrid square tube and its energy absorption capability. *Composite structures*. 2002;57(1-4):279-287.
11. Jacob GC, Fellers JF, Simunovic S, Starbuck JM. Energy absorption in polymer composites for automotive crashworthiness. *Journal of composite materials*. 2002;36(7):813-850.
12. Kumar D, Kamle S, Mohite PM, Kamath GM. A novel real-time DIC-FPGA-based measurement method for dynamic testing of light and flexible structures. *Measurement Science and Technology*. 2019/03/18 2019;30(4):045903. doi:10.1088/1361-6501/ab01a7
13. Mahesh, Rawat P, Sai L, Behera RP, Singh KK, Zhu D. Shear performance of MWCNTs modified single-lap joints of glass/epoxy laminates. *Journal of Adhesion Science and Technology*. 2022/11/17 2022;36(22):2418-2437. doi:10.1080/01694243.2021.2011825
14. Audacity® software is copyright © 1999-2021 Audacity Team. Web site: <https://audacityteam.org/>. It is free software distributed under the terms of the GNU General Public License. The name Audacity® is a registered trademark. <https://audacityteam.org/>
15. Thompson DE. An Overview of Audacity. *General Music Today*. 2014/04/01 2014;27(3):40-43. doi:10.1177/1048371314523964
16. Guden M, Yüksel S, Taşdemirci A, Tanoğlu M. Effect of aluminum closed-cell foam filling on the quasi-static axial crush performance of glass fiber reinforced polyester composite and aluminum/composite hybrid tubes. *Composite structures*. 2007;81(4):480-490.
17. Sathishkumar T, Satheeshkumar S, Bhuvaneshkumar K, Sanjay M, Siengchin S. Crashworthiness characterization of jute fiber woven mat reinforced epoxy composite tube for structural application using Taguchi's method. *International Journal of Crashworthiness*. 2022;27(5):1351-1367.
18. Mirzaei M, Shakeri M, Sadighi M, Akbarshahi H. Experimental and analytical assessment of axial crushing of circular hybrid tubes under quasi-static load. *Composite structures*. 2012;94(6):1959-1966.

19. Quanjin M, Merzuki MNM, Rejab MRM, Noh MZC. Compressive behaviour of aluminium rectangular hollow tube using Digital Image Correlation (DIC) method. *IOP Conference Series: Materials Science and Engineering*. 2020/05/01 2020;863(1):012038. doi:10.1088/1757-899X/863/1/012038
20. Blaber J, Adair B, Antoniou A. Ncorr: open-source 2D digital image correlation matlab software. *Experimental Mechanics*. 2015;55(6):1105-1122.
21. Harilal R. Adaptation of open source 2D DIC software Ncorr for solid mechanics applications. 2014.